

X-ray satellite lines of high- n Rydberg transitions in Ar^{16+}

E. Källne

Department of Physics I, Royal Institute of Technology, S-100 44 Stockholm, Sweden

J. Källne

JET Joint Undertaking, Abingdon-on-Thames, OX14 3EA, United Kingdom

J. Dubau

Observatoire de Paris—Meudon, F-92190 Meudon Principal Cédex, France

E. S. Marmor and J. E. Rice

Massachusetts Institute of Technology Plasma Fusion Center, Cambridge, Massachusetts 02139

(Received 31 July 1987; revised manuscript received 8 March 1988)

The He-like spectrum of $1s^2-1snp$ transitions and satellites in Ar^{16+} have been measured from the plasma of the Alcator-C tokamak. In the wavelength region of $\lambda=3.0-3.4$ Å, three groups of satellite lines $1s^2\sigma-1s2\sigma nl$ are observed which accompany each of the resonance lines of the orbitals from $n=4$ to 10. The results of calculations presented were used for identification of the observed spectrum and for discussion of line intensities and wavelengths. Radial-scan measurements were also performed over plasma regions of different electron temperatures. It is shown that such data can be used for estimating the relative importance of dielectronic recombination and inner-shell excitation in the population of satellites.

I. INTRODUCTION

A common feature of x-ray spectra from highly ionized atoms is the presence of satellite lines.¹ For instance, the He-like spectrum of $n=2$ to $n=1$ transitions contains four principal lines, $1s^2-1s2p$ and $1s^2-1s2s$, and several known $1s^2\sigma-1s2\sigma 2l$ satellite lines besides a number of less well-characterized ones from $1sn\sigma 2l$ states of $n > 2$.² The isoelectronic sequence of such spectra has been much studied under the conditions presented by plasmas of electron densities in the range $N_e=10^{10}-10^{15}$ cm⁻³ and temperatures in the range $T_e=0.5-5$ keV. These conditions are, for instance, met in astrophysical plasmas as well as in tokamak plasmas in which ions occur with charge-state distributions close to those of corona equilibrium. For temperatures around and below the ionization potential for forming the He-like charge state, the He-like spectrum and its satellites are strongly populated and present suitable conditions for observations. Measurements up until now have covered the isoelectronic sequence up to $Z=28$, depending on plasma temperature, and have been performed either for the purpose of diagnosing the plasma or for studying the physics of highly ionized atoms.³⁻⁶ In the present experiment, T_e was about 1.5 keV which allowed the study of the He-like spectrum of argon.

While He-like spectra of the $n=2$ states have been extensively studied, rather few experiments have been published on the transitions from the higher-lying orbitals. This reflects in part the fact that x-ray lines of the $n=2$ states are the strongest ones and amenable to measurement while those of the higher-lying states are weaker (due to the decrease in excitation rates with increasing n) and the line energy separation is smaller. Still, some crystal spectrometer measurements have been reported

on the Rydberg series of transitions in He-like spectra for laser- and vacuum-spark-produced plasmas.⁷ High- n spectra have also been observed from solar flares with satellite-borne spectrometers.⁸ Ion-atom collisions in gas targets have been used to produce highly charged recoil ions whose spectra have revealed the excitation of high- n states and accompanying stabilizing x-ray transitions.⁹ In a previous paper,¹⁰ we have reported on measurements of the Rydberg series of ground-state transitions in He-like Ar from the plasma of the Alcator-C tokamak. This study demonstrated in particular the importance of the recombination population of the principal lines for states of high n . Here we shall concentrate on the satellites accompanying high- n resonance transitions in the He-like Ar spectrum involving excited states of the type $1s2\sigma nl$.

For the interpretation of the He-like spectra there have been several theoretical calculations of the satellites $1s^2\sigma-1s2\sigma nl$ for $n=2$.^{11,12} The $1s^2\sigma-1s2\sigma nl$ satellites of higher-orbital transitions have been predicted in connection with experiments on high-density laser-induced plasmas.⁷ In a recent calculation based on the Hartree-Fock model with relativistic corrections, the satellite spectra of transitions in Ar^{15+} from orbitals $n=3$ and 4 were presented.¹³ Here we present the results for transitions from orbitals $n=4$ and 5 obtained from calculations based on a similar multiconfiguration intermediate-coupling model,¹⁴ but using central-potential radial wave functions rather than the Hartree-Fock wave functions used in Ref. 13; the central potential is a scaled Thomas-Fermi-Dirac potential where the scaling parameter was determined self-consistently by an energy-minimization procedure. The satellites of each orbital can be classified in terms of transitions of the type $1s2\sigma(^{2S+1}L)nl \rightarrow 1s^2\sigma$ since they are structured largely according to the energy of the $1s2\sigma(^{2S+1}L)$ core of the

initial state and of the 2σ valence-electron state of the final state. For the higher orbitals $n \geq 4$, the result is a satellite spectrum consisting of a few groups of lines whose positions relative to the resonance line change very little with n thus approaching the situation of Rydberg transitions as n increases.

A main motivation for this work was the study of the satellite structure of the He-like spectra of Rydberg states. Comparison can be made with the situation in the $n=2$ spectrum where the energy spread within the groups is largely due to the residual interactions in the initial-state configuration. In the latter case the $1s^2n\sigma$ - $1s2ln\sigma$ satellites for $n=2$ and $n \geq 3$ are usually separated in energy with the $N \geq 3$ satellites appearing as unresolved features on the low-energy side of the $1s^2$ - $1s2p$ resonance line.¹⁵ Their counterparts in the high- n spectra ($1s^22\sigma$ - $1s2\sigma nl$) are well separated from the $1s^2$ - $1snp$ resonance lines so that information on the $1s2\sigma nl$ states can be gained by studying the satellite spectrum as a function of n . Another aspect to consider is that satellite interference hampers accurate measurements of absolute wavelengths, relative intensities, and line profiles of principal lines in $n=1$ He-like spectra. Since the decay of the $1sn_1\sigma n_2l$ states is almost exhausted by autoionization for $n_1 \geq 3$ and $n_2 \geq 3$ these problems can be avoided if this information can be obtained from $n > 3$ spectra. The spectral region of the high- n Rydberg states is also of interest since it contains the states that are preferentially populated in ion-atom collisions (such as charge exchange with neutral hydrogen), and perhaps in ion-ion collisions compared to electron-ion collisions which in hot-and low-density plasma always dominates the population of the lowest excited states of highly ionized atoms.

II. EXPERIMENTAL

The measurements were made with a Bragg crystal spectrometer at the Alcator-C tokamak. This type of measurement has been described before¹⁶ and only information pertinent for this experiment is given here. Argon was introduced into the plasma of hydrogen in a small amount which was adjusted to obtain the desired count rate. The count rate had to approach the level of 10^5 counts/s for the strongest lines in order to see the weakest ones of interest; a dynamic range of about 10^3 was required. The plasma had typically an electron temperature of $T_e = 1.5$ keV in the center and a density of $n_e = 2 \times 10^{14}$ cm⁻³ for Ohmically heated discharges in hydrogen; electrons and ions can be assumed to have thermal (Maxwellian) velocity distributions. The plasma was limited by an aperture with a radius of 16.5 cm. The electron temperature is a rapidly decreasing function of radius, approximately described by $T_e(r) = T_0 \exp^{-(r/9)^2}$ for our plasma discharges with the minor radius r in centimeters. The plasma was viewed perpendicular to the plasma toroidal axis and the line of sight was usually through the center. Some measurements, however, were also made along chords at a variable distance d from the center with d in the range $0 < d < 10$ cm.

Spectra were recorded during the quasisteady state of the discharge being typically 200 ms. The spectrometer

bandwidth was about 1.5% for a given Bragg-angle setting and successive settings were used to cover the wavelength range of 3.0 to 3.4 Å. A change in the spectrometer setting was made between discharges and the data needed for constructing composite spectra were accumulated by repetition of similar discharges. The spectrometer wavelength resolution was about 1:2500. The observed line profiles were essentially Gaussian with a width of about 1:1500 whose main contribution was attributable to Doppler broadening at ion temperatures of about 1.2 keV. All wavelength determinations were made relative to the well-known principal lines of the $1s^2$ - $1snp$ Rydberg series of transitions in Ar¹⁶⁺; the formula [Eq. (1) of Ref. 8] was used as reference wavelength scale.

III. THEORETICAL BACKGROUND

In the center of tokamak plasmas, one can find conditions for which the ionic charge distribution is close to that of corona equilibrium and the electron energy distribution is Maxwellian. At an electron temperature of $T_e = 1.5$ keV, the resonance lines of Ar¹⁶⁺ ($1snp$ 1P_1 - $1s^2$ 1S_0 , denoted w_n as in Ref. 2) are then strongly populated by electron-impact excitation



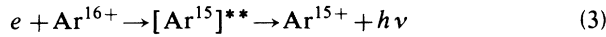
These resonance lines are the main Ar¹⁶⁺ lines in the x-ray spectra of $n \geq 3$ while the $n=2$ spectrum also contains other intense principal lines: the intercombination lines (conventionally² denoted x and y) and the forbidden line (z) connected with the states $1s2p$ $^3P_{2,1}$ and $1s2s$ 3S_1 , respectively. The intensity of w_n is proportional to the electron and Ar¹⁶⁺ density numbers (N_e and $N_{Ar^{16+}}$), and to the excitation rate $C_{w_n}(T_e)$ which varies through the Rydberg series

$$I_{w_n} = N_e N_{Ar^{16+}} C_{w_n}(T_e) \propto \frac{1}{n^3} \frac{N_e N_{Ar^{16+}}}{T_e^{1/2}} \exp \left[-\frac{E_n}{kT_e} \right] . (2)$$

The approximate expression in Eq. (2) is obtained using the van Regemorter formula¹⁷ where E_n is the excitation energy corresponding to the transition w_n .

For the x-ray emission emanating from peripheral regions of the plasma, other population mechanisms can compete with electron-impact excitation. This is especially true for higher- n states due to the decrease in the impact excitation rate with E_n giving increased relative importance to radiative and charge-exchange recombination involving Ar¹⁷⁺. The crucial condition for this to happen is an increase of the Ar¹⁷⁺-to-Ar¹⁶⁺ abundance ratio which is higher than the corona equilibrium; this is indeed found to be the case in peripheral plasma regions because of ion transport effects as discussed previously.^{10,18} Under these circumstances, the observed resonance line intensity will fall less rapidly with increasing n than is given by the above expression for impact excitation.

The satellite lines are mainly populated by dielectronic recombination



and it is the indicated radiative decay branch of the autoionizing state $[\text{Ar}^{15+}]^{**}$ that is observed in the x-ray spectra; the asterisks indicate an inner-shell excited (singly or doubly) state involving a high- n orbital ($n \geq 3$) while Ar^{16+} indicates that the ion is in its ground state, $1s^2$. The radiative decay occurs in competition with the autoionization (rate coefficient A_a) and other radiative decays (A_r) so that the dielectronic satellite intensity belonging to the initial upper state i and the final state f can be expressed as

$$I_{if}^s(T_e) = N_e N_{\text{Ar}^{16+}} F_2^*(if) F_1^*(i, T_e), \quad (4)$$

where

$$F_2^*(if) = g_i \frac{A_a^i A_r^{if}}{A_a^i + \sum_{f'} A_r^{if'}}, \quad (5)$$

$$F_1^*(i, T_e) = \frac{1}{2} \left[\frac{h^2}{2\pi m k T_e} \right]^{3/2} \exp \left[-\frac{E_i^s}{k T_e} \right]; \quad (6)$$

here g_i is the statistical weight of the autoionizing state i and E_i^s is the energy of this state relative to the He-like Ar^{16+} ground state. The energies of the doubly excited states $1s2\sigma nl$ for $n=4$ and 5 were computed in the present work and found to be distributed over a few narrow energy bands around $E_4^s = 2904$ and $E_5^s = 2984$ eV, respectively. In order to obtain the general n dependence of the energies E_n^s and E_n , we use the approximate expressions

$$E_n^s = E_2 - \frac{(Z-2)^2}{n^2} E_R \quad (7)$$

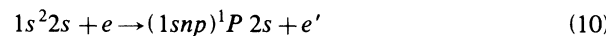
and

$$E_n = \left[(Z-0.6)^2 - \frac{(Z-1)^2}{n^2} \right] E_R, \quad (8)$$

where Z is the argon nuclear charge ($Z=18$) and E_R is the Rydberg energy ($E_R = 13.606$ eV). Hence, the energy and temperature dependences of the satellite-to-resonance-line intensity ratio can be expressed as

$$\left[\frac{I_{if}^s}{I_w} \right]_n \propto \frac{1}{T_e} \exp \left[\frac{E_n - E_n^s}{k T_e} \right]; \quad (9)$$

it is assumed that the resonance line is populated by impact excitation only. While most of the autoionizing states of Ar^{15+} are usually strongly populated through dielectronic recombination with the $1s^2 1S_0$ ground state of Ar^{16+} (dielectronic satellites), some of these states can also be reached by inner-shell excitation of the Ar^{15+} ground state



(inner-shell satellites). Clearly, this excitation process is similar to that for the resonance line w_n since the $2s$ electron is mostly a spectator in the excitation. However, the upper state of configuration $(1snp)^1 P 2s$ is not an (energy) eigenstate but is strongly mixed with $(1snp)^3 P 2s$ and oth-

er $1s2\sigma nl$ configurations in the same complex. For large n , these states are therefore better characterized according to their core configurations $1s2s(^1S_0)nl$ and $1s2s(^3S_1)nl$ since mixing of these configurations decreases with increasing n ; generally we will refer to these dominant configuration states by $1s2\sigma(^{2S+1}L)nl$ which converge to the true eigenstates at the ionization limits. Assuming that the impact excitation of the $1s^2 2s$ and $1s^2$ states is basically the same, we can use recoupling coefficients (or simple statistical arguments) to obtain estimates for the excitation rates of the states $(1s2s)^1 S(np)^2 P$ and $(1s2s)^3 S(np)^2 P$ which are $C_w/4$ and $3C_w/4$, respectively. These estimates are only approximate but should work rather well for highly charged ions and large- n values where multiconfiguration expansion effects of the wave functions are known to disappear. Since the $^2 P$ terms are split by a spin-orbit interaction into $^2 P_{1/2}$ and $^2 P_{3/2}$, the excitation rates of the corresponding levels are obtained by multiplying the term excitation rates by $\frac{1}{3}$ and $\frac{2}{3}$, respectively. The intensity of inner-shell satellites, I_{if}^s , relative to the w_n resonance-line intensity can be expressed as

$$\frac{I_{if}^s}{I_{w_n}} = \frac{N_{\text{Ar}^{15+}}}{N_{\text{Ar}^{16+}}} M \frac{A_r^{if}}{A_a^i + \sum_{f'} A_r^{if'}}, \quad (11)$$

where M is the multiplicative factor described above; this line ratio varies with electron temperature through the density ratio.

Since the population of satellites involves the excitation of the Ar^{16+} ground state, radiative and charge-exchange recombination by Ar^{16+} (involving thermal electrons and hydrogen atoms, respectively) can usually not contribute. Although the double charge exchange $\text{He} + \text{Ar}^{17+} \rightarrow [\text{Ar}^{15+}]^* + \text{He}^{2+}$ in a helium plasma could, in principle, populate states of the type $1s2\sigma nl$, the effect on the observed He-like x-ray spectrum would be negligible because high- n states with $n_1 \approx n_2$ would be preferentially populated and the neutral helium density is small in the plasma. Therefore, when radiative or (single) charge-exchange recombination processes on Ar^{17+} do contribute to the population of the resonance lines of the He-like spectrum, the measured I_s/I_w will fall below the ratio given by the expression given above. This is known¹⁸ to happen in the plasma periphery so that satellites can be identified by the observation of a rapid decrease in line intensity relative to the resonance line with increasing plasma radius.

The dielectronic satellite spectrum of transitions from $n=4$ and 5 in Ar^{16+} were calculated using the numerical methods (minimization procedures, potential scaling parameters, etc.), and the programs SUPERSTRUCTURE and AUTOLSJ described elsewhere.¹⁴ This model is especially suitable for calculation of extensive atomic data since a common set of mono-electronic wave functions ($1s, 2s, 2p, 3s, 3p, 3d, 4s, 4p, 4d, 4f, 5s, 5p, 5d, 5f$) is used to construct Slater determinants for the many-body wave functions; altogether 38 configurations, $1s^2 2l'$, $1s 2l' n l$ with $n \leq 5$ and $l \leq 3$, were considered in these calculations. Although the obtained wavelength accuracy of

about $\Delta\lambda/\lambda \approx 10^{-3}$ is not sufficient for identifying the experimental spectra, the relative accuracy is much better ($\ll 10^{-3}$) for similar transitions (e.g., parent and satellite lines) where cancellation of common errors occur. The results on wavelengths (using the same reference as stated in Sec. II) and relative satellite intensities (as well as relevant rate information) are presented in Tables I and II; these results were obtained from the computer code as previously used for the results presented in Ref. 14. For the $n=4$ orbital, comparison is made with the calculation of Bhalla and Tunnel;¹³ in Table I we, therefore, have given the coupling schemes of both models to show the transition identifications made. Good agreement is found with regard to both wavelengths and transition rates as well for the relative dielectronic satellite intensities; the satellite intensities given in column 7 of Table I were deduced from the data given in Ref. 11.

IV. EXPERIMENTAL RESULTS

A. Spectral line structure

An example of a measured spectrum for the wavelength range 3.0 to 3.4 Å is shown in Fig. 1. It is dominated by the series of $1s^2-1snp$ transitions with principal quantum numbers n from $n=3$ up to the series limit occurring at $E=4.120$ keV or $\lambda=3.0088$ Å;⁸ the $n=2$ to $n=1$ He-like spectrum has been measured for similar plasma conditions earlier.¹⁰ These principal lines of the He-like spectrum have been discussed in detail previously with regard to different population mechanisms (viz., electron-impact excitation, radiative recombination, and charge-transfer recombination with neutral hydrogen) and their dependence on the conditions in different plasma regions.^{10,18} The spectrum shown is dominated by emission from the plasma center (central line of sight) where the electron temperature is about 1.5 keV and the

predominant population mechanism is electron-impact excitation. The variation in intensity is more than 2 orders of magnitude over the range $n=3$ to 10 and follows approximately (Fig. 2) the expected $1/n^3$ dependence of Eq. (1).

On the long-wavelength side of the $n=3$ resonance line, there appears a weak line which can be identified with the intercombination transition (y_3) of the $1s3p\ ^3P_1$ state; it is found to be separated by 3.5 mÅ from the resonance line (w_3) with an intensity ratio of $I_{y_3}/I_{w_3}=0.08$ which is in agreement with predictions.¹⁹ The ground-state x-ray transition from the other spin state ($1s3p\ ^3P_2$) of the same term is merged with the resonance line and is of insignificant relative intensity; for $n>3$, both intercombination lines are predicted to be negligible. One may also notice the presence of a line at $\lambda=3.150$ Å which is due to the $1s-3p$ transition of Ar¹⁷⁺.

The remaining features of the spectrum in Fig. 1 can be ascribed to satellite lines. A set of three groups (called S1, S2, and S3) can be identified as satellites of the $n=4$ resonance line. The satellite groupings can be followed through the transition series of increasing n towards the series limit at $\lambda=3.0938$ Å for S3_∞. However, as the series limit is approached, the line density increases and the intensities are weaker relative to the background so that no satellites are resolvable for orbitals with $n>10$. The satellites of the $n=3$ resonance transition were outside the range of the present measurement. However, some of these satellites have been observed in sulphur earlier for similar plasma conditions²⁰ as have those of the He-like $n=2$ spectrum of argon^{4,14} which will be discussed later.

The observed satellite groupings are identified in terms of transitions $1s^22\sigma-1s2\sigma nl$ in Ar¹⁵⁺ with the help of the theoretically predicted wavelengths and relative intensities given in Tables I and II for the $n=4$ and 5 satellites spectra; lines of intensity lower than 5% of the strongest

TABLE I. Ar XVI $n=2$ dielectronic satellites of $1s4p-1s^2$. The 12 strongest lines are given and identified by their upper and lower states, and by groups, with the calculated results on wavelength (λ), autoionization rate (A_a), radiative rate (A_r), and line intensity (F_2^*); the rates are in units of 10^{14} s⁻¹. Comparison is made with the theoretical results of Ref. 13; complementary upper-state information is given where necessary.

Line no.	Array	Key	Bhalla and Tunnel (Ref. 13)				Present work			
			λ (Å)	A_a	A_r	$F_2^*(if)$	λ (Å)	A_a	A_r	$F_2^*(if)$
1	$1s2s(^1S)4p\ ^2P_{1/2}-1s^22s\ ^2S_{1/2}$ [$1s4p(^3P)2s$]	S1 ₄	3.2440	1.771	0.209	0.305	3.2438	1.570	0.157	0.211
2	$1s2s(^1S)4p\ ^2P_{3/2}-1s^22s\ ^2S_{1/2}$ [$1s4p(^3P)2s$]	S1 ₄	3.2445	0.124	0.236	0.174	3.2442	0.142	0.287	0.174
3	$1s2s(^3P)4s\ ^2P_{1/2}-1s^22s\ ^2S_{1/2}$	S1 ₄	3.2461	0.176	0.105	0.097	3.2453	0.140	0.161	0.108
4	$1s2s(^3S)4p\ ^2P_{1/2}-1s^22s\ ^2S_{1/2}$ [$1s4p(^1P)2s$]	S2 ₄	3.2611	0.199	0.751	0.276	3.2599	0.198	0.829	0.316
5	$1s2s(^3S)4p\ ^2P_{3/2}-1s^22s\ ^2S_{1/2}$ [$1s4p(^1P)2s$]	S2 ₄	3.2612	0.199	0.735	0.547	3.2600	0.208	0.815	0.649
6	$1s2p(^1P)4p\ ^2D_{5/2}-1s^22p\ ^2P_{3/2}$	S3 ₄	3.2605	0.895	0.256	0.118	3.2600	0.991	0.329	0.168
7	$1s2p(^3P)4p\ ^2D_{3/2}-1s^22p\ ^2P_{1/2}$	S3 ₄	3.2691	0.511	0.135	0.229	3.2680	0.671	0.142	0.254
8	$1s2p(^3P)4p\ ^2S_{1/2}-1s^22p\ ^2P_{3/2}$	S3 ₄	3.2692	0.354	0.669	0.309	3.2686	0.398	0.783	0.384
9	$1s2p(^3P)4p\ ^2P_{3/2}-1s^22p\ ^2P_{1/2}$	S3 ₄	3.2707	0.548	0.583	0.915	3.2697	0.584	0.658	1.082
10	$1s2p(^3P)4p\ ^2D_{5/2}-1s^22p\ ^2P_{3/2}$	S3 ₄	3.2704	1.455	0.678	2.549	3.2699	1.345	0.666	2.612
11	$1s2p(^3P)4f\ ^4G_{5/2}-1s^22p\ ^2P_{3/2}$	S3 ₄	3.2710	0.142	0.075	0.131	3.2704	0.212	0.148	0.473
12	$1s2p(^3P)4p\ ^2D_{3/2}-1s^22p\ ^2P_{3/2}$	S3 ₄	3.2719	0.591	0.442	0.754	3.2714	0.671	0.525	0.938

TABLE II. Ar XVI $n=2$ dielectronic satellite of $1s5p-1s^2$. The eight strongest satellites are given and identified by their upper and lower states, and by group, with the calculated results on wavelength (λ), autoionization rate (A_a), radiative rate (A_r), and line intensity (F_2^*); the rates are given in units of 10^{14} s^{-1} .

Line No.	Array	Key	λ (Å)	A_a	A_r	F_2^* (if)
1	$1s2s(^1S)5p^2P_{1/2}-1s^22s^2S_{1/2}$	S1 ₅	3.1765	0.649	0.199	0.120
2	$1s2s(^1S)5p^2P_{3/2}-1s^22s^2S_{1/2}$	S1 ₅	3.1765	0.246	0.144	0.172
4	$1s2s(^3S)5p^2P_{1/2}-1s^22s^2S_{1/2}$	S2 ₅	3.1922	0.149	0.440	0.221
5	$1s2s(^3S)5p^2P_{3/2}-1s^22s^2S_{1/2}$	S2 ₅	3.1922	0.150	0.431	0.440
8	$1s2p(^3P)5p^2S_{1/2}-1s^22p^2P_{3/2}$	S3 ₅	3.2022	0.240	0.436	0.264
9	$1s2p(^3P)5p^2P_{3/2}-1s^22p^2P_{1/2}$	S3 ₅	3.2022	0.506	0.395	0.761
10	$1s2p(^3P)5p^2D_{5/2}-1s^22p^2P_{3/2}$	S3 ₅	3.2029	0.841	0.393	1.602
12	$1s2p(^3P)5p^2D_{3/2}-1s^22p^2P_{3/2}$	S3 ₅	3.2035	0.188	0.305	0.428

one were not considered. In the theoretical $n=4$ spectrum there are altogether 12 such satellites forming three groups separated by 44, 62, and 72 mÅ, respectively; these values are the weighted means of the contributing lines. The internal wavelength spread within the group is less than 2.0 mÅ which, if expressed as the full width at

half maximum (FWHM) of an equivalent Gaussian distribution, is comparable to the width observed of well-resolved individual lines in the measured spectrum (see Sec. II). The same general satellite structure of relative wavelengths and intensities is predicted for the $n=5$ orbital which is also in agreement with the measurement

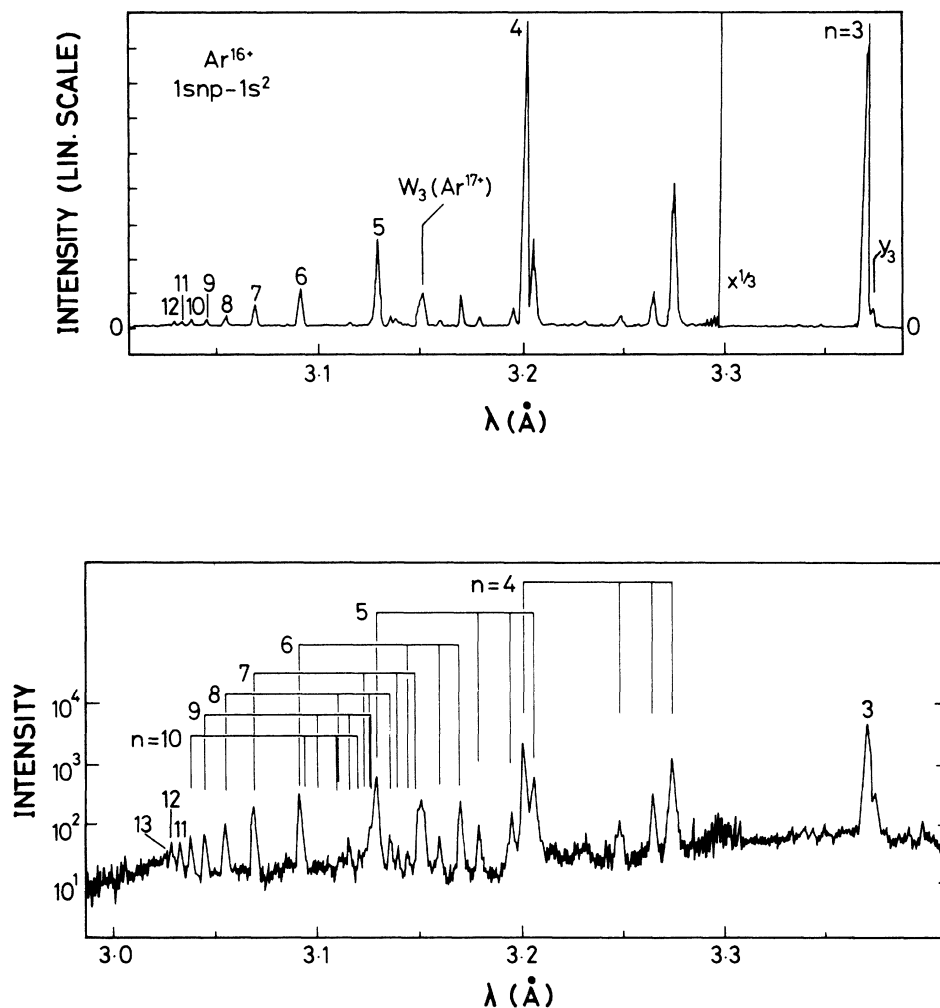


FIG. 1. The measured He-like spectrum of Ar. The $1snp\ ^1P_1-1s^2\ ^1S_1$ resonance lines (w_n) and accompanying satellites (S1_n, S2_n, and S3_n) are indicated as well as the $1s3p\ ^3P_2-1s^2\ ^1S_1$ intercombination line (X_3), the $1s-3p$ resonance line of H-like Ar (w_3).

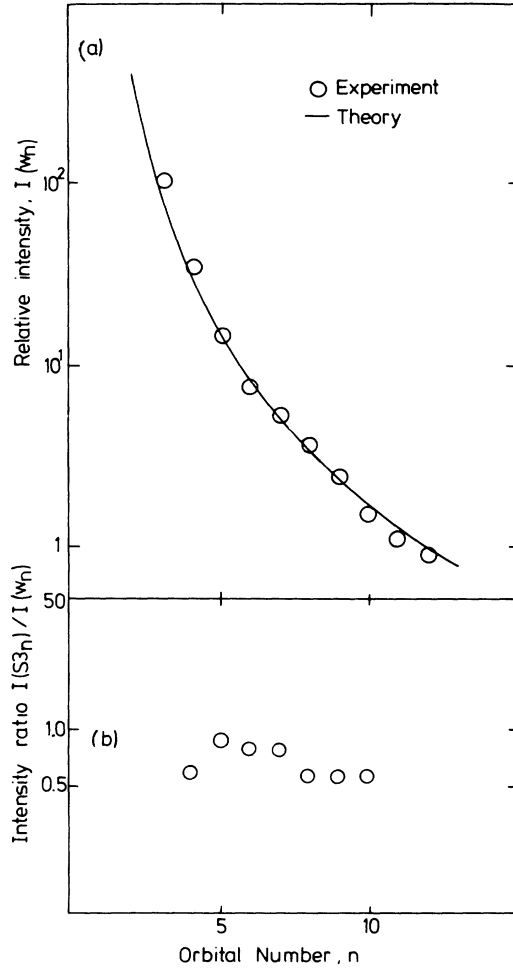


FIG. 2. The measured relative intensity variation of the $1snp-1s^2$ resonance lines $w_n(a)$ and of the intensity ratio $I(S3_n)/I(w_n)$ of the satellite-to-resonance line as function of orbital number n ; comparison is made in (a) with the estimated n dependence of Eq. (2).

(Fig. 1 and Table III). For interpreting the $n \geq 5$ transition spectrum, we relied on small systematic changes in relative satellite intensities (I_s/I_w) (Fig. 2) and wavelength separations (Fig. 3) of $S1_n$, $S2_n$, and $S3_n$ as a function of n . Figure 2 and Table IV show the variations of the $S3_n$ groups relative to the resonance lines w_n ; there is no obvious variation with n which is also borne out by

the estimated values for a Rydberg series of transitions [Eq. (9)]. Although not all intensities of the high- n satellites were uniquely identified because of the unfolding problems, the identifications made fit into the Rydberg series systematics. Thus, all significant intensities of the observed spectrum have been identified with satellited groups for resonance lines up to $n = 10$ and with the principal lines mentioned earlier. The results on wavelengths and intensities are summarized in Tables III and IV and Figs. 2 and 3.

B. Spectra from different plasma regions

Some examples of measured satellite intensities as function of line of sight through the plasma are shown in Fig. 4. The intensity ratio of the $S3_4$ satellite group to the w_4 resonance line, $I(S3_4)/I(w_4)$ is found to increase with increasing distance d from the plasma center. This can be attributed to the plasma temperature profile (see Sec. II) and the temperature dependences of population by dielectronic recombination and electron-impact excitation [Eq. (9)]. However, in the plasma periphery, the radial dependence of $I(S3_4)/I(w_4)$ changes into a rapid decrease with increasing d ; which is caused by the onset of radiative or charge-exchange recombination contributions to the population of the resonance line. This is a typical gross behavior of the intensity ratios of satellite to resonance lines and is also shown by the data on the radial dependence of $I(S2_4)/I(w_4)$. In the central region of the plasma, however, the two satellite groups $I(S1_4)$ and $I(S2_4)$ show some differences. This could indicate that the radial dependence of satellite intensity ratios is sensitive to inner-shell excitation contributions since some satellite lines of the $S2_4$ group, are populated not only by dielectronic recombination but also by inner-shell excitation.

Comparison can be made with results on the $n=2$ spectrum obtained in a previous experiment¹⁸ from which we choose the satellites k and q that are populated by dielectronic recombination and (97% pure) inner-shell excitation, respectively (see Sec. V for more spectroscopic details). The line intensity ratio $I(k)/I(w_2)$ show the same general behavior as $I(q)/I(w_2)$. However, the $I(q)/I(w_2)$ ratio has a faster rise with increasing d in the central plasma region which is in close resemblance with the difference between the $I(S2_4)/I(w_4)$ and $I(S3_4)/I(w_4)$ ratios for the $n=4$ spectrum. One can also note

TABLE III. Results on wavelengths relative to the resonance line ($\Delta\lambda$) and (I) intensities for Ar XVI $n=2$ $1s4p-1s^2$ and $1s5p-1s^2$ satellites from measurements and calculations.

Satellite line	Expt.		Theory		
	$\Delta\lambda$ (mÅ)	I_{rel}	$\Delta\lambda$	I	I_{rel}
S1 ₄	46	9	46.8	0.49	9
S2 ₄	62	22	62.8	1.13	20
S3 ₄	71.2	100	72.8	5.74	100
S1 ₅	51.3	14	51.0	0.29	10
S2 ₅	66.5	26	66.7	0.68	22
S3 ₅	76.6	100	77.2	1.96	100

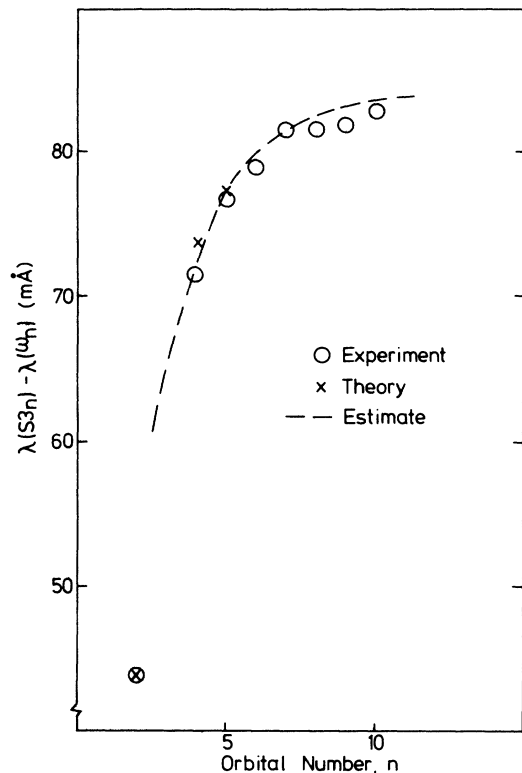


FIG. 3. The measured separation in wavelength $\lambda(S_{3_n}) - \lambda(w_n)$ between the satellite groups S_{3_n} and the resonance lines w_n as function of n . Comparison is made with theoretical values for $n=2, 4$, and 5 and with Rydberg-state estimates [Eqs. (7) and (8)].

an indication of an n dependence in these data on $n=2$ and $n=4$ spectra. The maximum of the $I(S_n)/I(w_n)$ as a function of d can be seen to move towards smaller d for higher- n values while the peak value tends to decrease. These features are all consistent with the radial temperature variation in the plasma [$T_e(r)$ as stated in Sec. II] and the temperature dependence of the satellite to resonance line ratio [as expressed by Eq. (9)]; in other words the relative satellite intensities become suppressed at the onset of recombination contributions to the resonance

line (which happens at higher temperatures and hence smaller d values for the high- n orbitals because the electron-impact excitation rates are then smaller). Of most interest to us here, however, is the radial variation of the $I(S)/I(w)$ intensity ratio which provides a clear signature for identifying satellite transitions relative to the principal lines and an indication as to the type of satellite (dielectronic or inner-shell satellite).

V. DISCUSSION

The satellite structure of He-like spectra consists of 12 significant lines as is shown by the $n=4$ spectrum. Most of the intensity is carried by nine transitions (Table I from upper-state configurations $1s2s(^1S)4p$, $1s2s(^3S)4p$, and $1s2p(^3P)4p$, as shown in Table V. These states are split in energy forming the satellite groups S_{1_4} , S_{2_4} , and S_{3_4} , respectively. Two of the satellite groups (S_{1_4} and S_{2_4}) are ground-state transitions separated in energy according to the basic electron configurations of the upper state (triplet-singlet energy splitting). The 2^1S and 2^3P states are almost degenerate so the separation of the S_{1_4} and S_{3_4} groups is due to the $2s$ and $2p$ energy difference of the final states ($1s^22p P_{1/2,3/2}$ and $1s^22s S_{1/2}$, respectively). The remaining three lines (lines 3, 6, and 11 in Table V) fall into the same energy bands because of circumstances as will be discussed later. This structure of resonance line and satellite peaks is repeated for other orbitals n and the He-like spectrum appears as a Rydberg series of transitions since, for increasing n , the interaction between the outer electron and the core electrons does not change very much. For lower n , however, the state dependence of satellite energies becomes important but still the first nine satellites observed in the present $n=4$ spectrum can be linked to counter parts in the commonly studied spectrum of $n=2$ transitions.

A comparison of the $n=2$ and 4 spectra, as obtained in a previous¹⁸ and in the present experiment under similar plasma conditions, is shown in Fig. 5. The $n=2$ spectrum consists of the resonance line (upper state 1P_1) and three other principal lines 3P_2 , 3P_1 , and 3S_1 . However, in the $n=4$ spectrum appears only the resonance line while the ground-state transitions of the 4^3P and 4^3S states are not seen because of the much larger rates for the compet-

TABLE IV. Results on measured relative intensities of the satellite groups S_{1_n} , S_{2_n} , and S_{3_n} , and the resonance lines w_n for $1snp-1s^2$ transitions.

Orbital n	Resonance line intensity w	$I(S_{1_n})/I(w_n)$		Relative Satellite intensities		
		w	S3	S3	S2	S1
3	1000					
4	350	100	58	100	22	8
5	142	100	90	100	26	15
6	77	100	82	100	19	10
7	52	100	78	100	21	
8	35	100	56	100		
9	23	100	55	100		
10	15	100	52	100		
11	12					

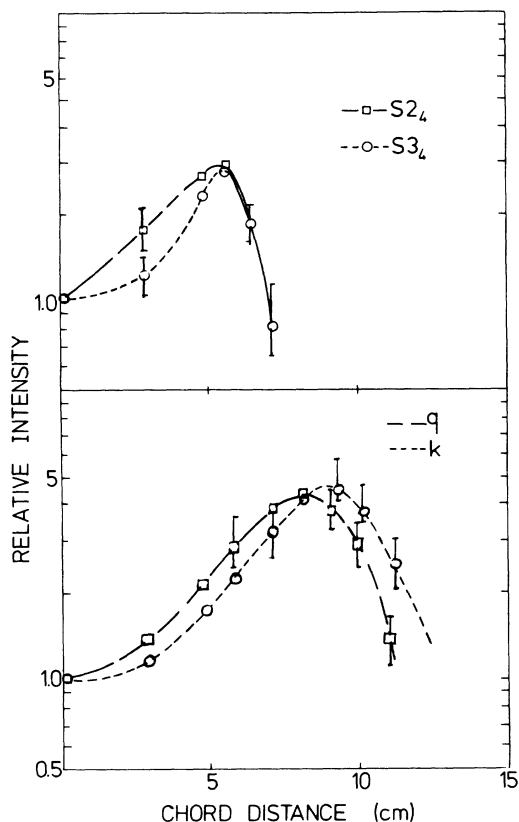


FIG. 4. The measured relative line intensities for different lines of sight through the plasma expressed as the chord distance d from the plasma center. Shown are data on $I(S_{3_4})/I(w_4)$ and $I(S_{2_4})/I(w_4)$ and those on $I(k)/I(w_2)$ and $I(q)/I(w_2)$ (taken with a 16.5-cm limiter radius). The experimental uncertainties (marked with error bars in the figure) are typically $\pm 20\%$ for S_{2_4} and S_{3_4} , and $\pm 10\%$ for k and q . The data points have been normalized at the plasma center (ratio=1). The k and q lines represent almost pure satellite population by dielectronic recombination and inner-shell excitation, respectively.

ing dipole transitions to states of $n \geq 2$.

With regard to satellites, the $1s2s(^3S_1)4p^2P_{1/2,3/2} - 1s^22s^2S_{1/2}$ transitions of the S_{2_4} satellite group have counterparts in the $n=2$ spectrum commonly known as the q and r lines (cf. also Table V). Similarly, the strong-

est transitions of the S_{3_4} group are of the type $1s2p(^3P)4pL_j - 1s^22pP_{1/2,3/2}$ (where $L_j = S_{1/2}, P_{3/2}, D_{3/2},$ or $D_{5/2}$) which correspond to the lines ($m, b, a, k,$ and j) in the $n=2$ spectrum; some of these lines are blended with other lines in the He-like spectrum of argon but have been seen as predicted for other ions in the He-like isoelectronic sequence.⁴⁻⁶ The S_{1_4} group contains dominant transitions of the configurations $1s2s^1S_0(4pP_{1/2,3/2} - 1s^22sS_{1/2})$ which correspond to the known s and t satellites in the $n=2$ spectrum although they are relatively too weak to be resolved in the measured Ar spectrum. This comparison illustrates that the rather complex structure of the $n=2$ spectrum transforms, for spectra of $n=4$ and higher orbitals, into one resonance line and three satellite groups; i.e., the state-dependent energy shifts of the lines, which in the $n=2$ spectrum are comparable to the differences in energy between the electron configurations (in terms of electron orbitals and spin interactions), are small for $N \geq 4$ spectra.

Besides the nine satellites mentioned above, there are three additional ones peculiar to the n value of the transition. The $1s2p(^1P)4p^2D_{5/2} - 1s^22p^2P_{3/2}$ transition (making specific reference to the $n=4$ spectrum as shown in Table V) is the only $n=4$ to $n=1$ transition from the 1P state that is not pre-empted by the very fast $1s2p4p - 1s^24p$ decay branch. This transition falls energetically within the S_{2_4} satellite group so that the $S_{2_4} - S_{3_4}$ separation is an approximate measure of the $^1P - ^3P$ spin splitting. The upper states of the transitions $1s2p(^3P)4s^2P_{1/2} - 1s^22s^2S_{1/2}$ and the $1s2p(^3P)4fG_{5/2} - 1s^22p^2P_{3/2}$ are nearly degenerate with the $1s2s(^3S)4p$ and the $1s2p(^3P)4p$ states, respectively, and both decay by dipole radiation as allowed through configuration mixing with the latter states; for higher orbitals other higher angular momentum states can be admixed and fast ground-state transitions would be similarly allowed. Due to the degeneracy, these transitions end up in the satellite groups S_{1_4} and S_{3_4} , respectively. It is interesting to note that the satellite spectrum for $n \geq 4$ transitions mirrors the He-like $1s2l$ level diagram (and hence the corresponding $n=2$ x-ray spectrum of principal lines) if allowance is made for the $1s^22\sigma$ and $1s^22p$ energy shift of about 33 eV. Moreover, the strengths of the $n=4$ satellites are a reflection of the inverse of the decay rates of the He-like

TABLE V. The principle structure of the Ar XVI $n=2$ $1s4p-1s^2$ satellites identified by group, line number, and transition array (considering the main term only). Comparison is made with corresponding $1s2p-1s^2$ lines identified by conventional letter symbols.

Satellite group	Lines		Transition
	$n=4 \rightarrow n=1$	$n=2 \rightarrow n=1$	
S1	1,2	s, t	$1s2s(^1S_0)4pP_{1/2,3/2} \rightarrow 1s^22s^2S_{1/2}$
S1	3		$1s2p(^3P)4s^2P_{1/2} \rightarrow 1s^22s^2S_{1/2}$
S2	4,5	q, r	$1s2s(^3S_1)4p^2P_{1/2,3/2} \rightarrow 1s^22s^2S_{1/2}$
S3	7,8,9 10,12	k, b, a, j, m	$1s2p(^3P)4p^2S_{1/2} \rightarrow 1s^22p^2P_{1/2,3/2}$
			$1s2p(^3P)4p^2S_{3/2} \rightarrow 1s^22p^2P_{1/2,3/2}$
			$1s2p(^3P)4p^2D_{3/2,5/2} \rightarrow 1s^22p^2P_{1/2,3/2}$
S2	6		$1s2p(^1P)4p^2D_{5/2} \rightarrow 1s^22p^2P_{3/2}$
S3	11		$1s2p(^3P)4fG_{5/2} \rightarrow 1s^22p^2P_{3/2}$

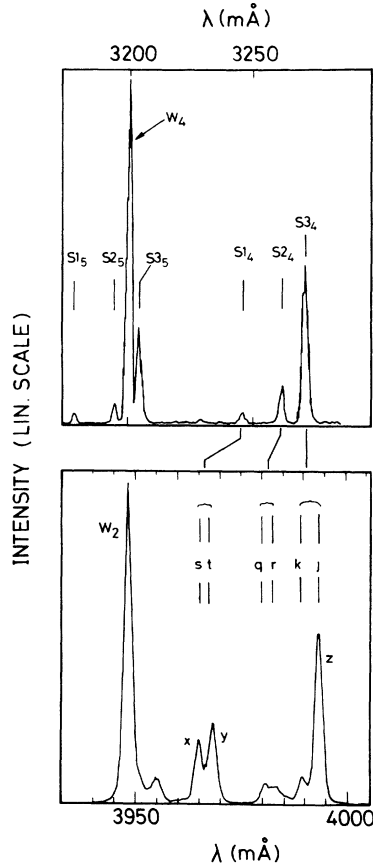


FIG. 5. Comparison of $n=4$ to $n=1$ and $n=2$ to $n=1$ transitions of the He-like Ar spectrum; the data are, respectively, from the present experiment and from Refs. 10 and 18 taken with a limiter radius of 16.5 cm. The line identifications are as in Table V.

$n=2$ to $n=1$ lines since these are competing decay branches; this means, for instance, that satellites based on the $1s2p(^1P)nl$ states appear with the weakest intensities.

In the $n=2$ spectrum (Fig. 5) there are significant satellite contributions (for instance, on the long-wavelength side of the resonance line) due to transitions from $1s2ln\sigma$ ($n \geq 3$) states. The $n > 2$ resonance lines, however (cf. Figs. 1 and 5) do not have any corresponding $n \geq 3$ satellites. Freedom from $n > 2$ satellites is a crucial advantage in precision measurements of absolute wavelengths.²¹ It also allows one to determine the line profile and hence the line Doppler broadening (from which the plasma ion temperature can be determined), as well as the resonance line intensity; the intensity ratio I_s/I_w can be used, for instance, to determine the plasma electron temperature [cf., Eq. (9)]. In this region of $n > 2$ transitions one can mea-

sure both the H-like spectrum (the $3p-1s$ transition) and the He-like spectrum ($1snp-1s^2$ transitions) with accompanying satellites even with a rather limited spectrometer bandwidth.

It is worth noting that by suitable choice of atomic number Z the $np-1s$ and the $1snp-1s^2$ and satellite transitions can be shifted relative to each other so as to obtain good separation between lines of interest. The $n > 2$ transitions can therefore be useful for plasma diagnostic applications allowing a two-way determination of electron temperature through the line intensity ratio $I(W)/I(w)$ (which is proportional to the abundance ratio of H-like and He-like ions and hence electron temperature dependent) and the I_s/I_w ratio [which is dependent on T_e through Eq. (9)]. The ion temperature determination would in this case be obtainable from several well-defined line profiles.

A price to pay is lower intensities of the $n \geq 3$ resonance lines with accompanying satellites. Furthermore, these measurements have to contend with a lower signal-to-background ratio than those for the $1s2p-1s^2$ lines; the background in this case is mostly continuous bremsstrahlung emission (and hence set by the plasma under study) while the signal can be increased as required by increasing the ion concentration up to the permissible impurity level for the plasma. The argon concentration for these measurements was less than 0.1% of the electron density.

VI. CONCLUSION

We have presented new measurements of $n=2$ satellites for Ar^{16+} $1snp-1s^2$ $n \geq 4$ from a tokamak plasma with a central temperature of about 1.5 keV. We find three distinctive groups of satellites ($S1_n$, $S2_n$, and $S3_n$) for each resonance line $1snp-1s^2$ of n between 4 and 10. These were identified with the help of atomic calculations as belonging to transitions of the type $1s2s(^1S_0)np-1s^22s$, $1s2s(^3S_1)np-1s^22s$, and $1s2p(^3P_1)np-1s^22p$, respectively. The n dependencies of intensities and wavelengths are discussed and comparisons were made with commonly studied He-like spectra of $1s2l-1s^2$ transitions. As expected, the transitions from high- n states are free from $n > 2$ satellite blending so this part of He-like or H-like spectra can provide distinct advantages in spectroscopic precision measurements. Finally, we have presented data on radial scan measurements which suggests that such information can help to distinguish between inner-shell excitation and dielectronic recombination contributions to satellite lines.

ACKNOWLEDGMENTS

This work was supported in part by the U.S. Department of Energy. The computations were carried out on the NAS9080 of CIRCE, Orsay, France.

¹B. Edlén and F. Tyrén, *Nature (London)* **143**, 940 (1939); A. H. Gabriel and T. M. Paget, *J. Phys. B* **5**, 673 (1972).

²A. H. Gabriel, *Mon. Not. R. Astron. Soc.* **160**, 99 (1972).

³TFR Group, M. Cornille, J. Dubau, and M. Loulergue, *Phys.*

Rev. A **32**, 3000 (1985).

⁴E. Källne, J. Källne, and A. K. Pradhan, *Phys. Rev. A* **32**, 467 (1983); E. Källne and J. Källne, in *Atomic Physics*, edited by H. Narumi and T. Shimamura (North-Holland, Amsterdam,

- 1987), Vol. 10, p. 395; E. Källne and J. Källne, *Phys. Scr.* **T17**, 152 (1987).
- ⁵F. Bombarda, R. Giannella, E. Källne, G. Tallents, F. Bely-Dubau, P. Faucher, M. Cornille, J. Dubau, and A. H. Gabriel, *Phys. Rev. A* **37**, 504 (1988).
- ⁶J. Dubau and S. Volonté, *Rep. Prog. Phys.* **43**, 199 (1980).
- ⁷V. A. Boiko, S. A. Pikuz, U. I. Safronova, and A. Ya Faenov, *Mon. Not. R. Astron. Soc.* **185**, 789 (1978); E. V. Aglitski and A. M. Panin, *Opt. Spektrosk.* **58**, 743 (1985) [*Opt. Spectrosc. (USSR)* **58**, 453 (1985)].
- ⁸J. F. Seely and U. Feldman, *Phys. Rev. Lett.* **54**, 1016 (1985).
- ⁹R. J. Maurer, R. L. Watson, and G. J. Pedrazzini, *Nucl. Instrum. Methods* **214**, 117 (1983); H. F. Beyer, R. Mann, F. Folkmann, and H. Mokler, *J. Phys. B* **15**, 3853 (1982).
- ¹⁰J. E. Rice, E. S. Marmor, J. Terry, E. Källne, and J. Källne, *Phys. Rev. Lett.* **56**, 50 (1986); J. E. Rice, E. S. Marmor, E. Källne, and J. Källne, *Phys. Rev. A* **35**, 3033 (1987).
- ¹¹F. Bely-Dubau, P. Faucher, L. Steenman-Clark, M. Bitter, S. von Goeler, K. W. Hill, C. Camhy-Val, and J. Dubau, *Phys. Rev. A* **26**, 3459 (1982).
- ¹²L. A. Vainshtein and U. I. Safronova, *At. Data Nucl. Data Tables* **21**, 49 (1978).
- ¹³C. P. Bhalla and T. W. Tunnell, *J. Quant. Spectrosc. Radiat. Transfer* **32**, 141 (1984).
- ¹⁴TFR Group, F. Bombarda, F. Bely-Dubau, P. Faucher, M. Cornille, J. Dubau, and M. Loulergue, *Phys. Rev. A* **32**, 2374 (1985).
- ¹⁵M. Bitter, S. von Goeler, K. W. Hill, R. Horton, D. Johnson, W. Roney, N. Sauthoff, E. Silver, and W. Stodiek, *Phys. Rev. Lett.* **47**, 921 (1981).
- ¹⁶E. Källne, J. Källne, J. E. Rice, and E. S. Marmor, *Phys. Scr.* **31**, 551 (1985).
- ¹⁷H. van Regemorter, *Astrophys. J.* **136**, 906 (1962).
- ¹⁸E. Källne, J. Källne, J. E. Rice, and E. S. Marmor, *Phys. Rev. Lett.* **52**, 2245 (1984).
- ¹⁹V. A. Boiko, A. Ya Faenov, S. A. Pikuz, I. Yu Skobelev, A. V. Vinogradov, and E. A. Yukov, *J. Phys. B* **10**, 3387 (1977).
- ²⁰E. Källne and J. Källne, in *X-Ray and Atomic Inner-Shell Physics, Oregon, 1982*, Proceedings of the International Conference on X-Ray and Atomic Inner-Shell Physics, AIP Conf. Proc. No. 94, edited by B. Crasemann (AIP, New York, 1982), p. 463.
- ²¹E. Källne, J. Källne, P. Richard, and M. Stöckli, *J. Phys. B* **17**, L115 (1984), E. S. Marmor, J. E. Rice, E. Källne, J. Källne, and R. E. LaVilla, *Phys. Rev. A* **33**, 774 (1986).